

Isovector giant monopole and quadrupole resonances in a Skyrme energy density functional approach with axial symmetry

Kenichi Yoshida^{1,*}

¹*Department of Physics, Kyoto University, Kyoto, 606-8502, Japan*

(Dated: March 2, 2022)

Background: Giant resonance (GR) is a typical collective mode of vibration. The deformation splitting of the isovector (IV) giant dipole resonance is well established. However, the splitting of GRs with other multipolarities is not well understood.

Purpose: I explore the IV monopole and quadrupole excitations and attempt to obtain the generic features of IV giant resonances in deformed nuclei by investigating the neutral and charge-exchange channels simultaneously.

Method: I employ a nuclear energy-density functional (EDF) method: the Skyrme–Kohn–Sham–Bogoliubov and the quasiparticle random-phase approximation are used to describe the ground state and the transition to excited states.

Results: I find the concentration of the monopole strengths in the energy region of the isobaric analog or Gamow–Teller resonance irrespective of nuclear deformation, and the appearance of a high-energy giant resonance composed of the particle–hole configurations of $2\hbar\omega_0$ excitation. Splitting of the distribution of the strength occurs in the giant monopole and quadrupole resonances due to deformation. The lower K states of quadrupole resonances appear lower in energy and possess the enhanced strengths in the prolate configuration, and vice versa in the oblate configuration, while the energy ordering depending on K is not clear for the $J = 1$ and $J = 2$ spin-quadrupole resonances.

Conclusions: The deformation splitting occurs generously in the giant monopole and quadrupole resonances. The K -dependence of the quadrupole transition strengths is largely understood by the anisotropy of density distribution.

I. INTRODUCTION

The response of a nucleus to an external field induces various modes of excitation, reflecting many-nucleon correlations and inter-nucleon interactions in the nuclear medium. Since the external fields are classified by quantum numbers, the collective modes of motion are selectively excited [1]; the nuclear response is characterized by the transferred angular momentum ΔL , spin ΔS , isospin ΔT , and particle number ΔN .

The isovector (IV) giant dipole resonance (GDR) represented as $\Delta L = 1, \Delta S = 0, \Delta T = 1, \Delta N = 0$ is one of the well studied collective vibrational modes of excitation among various types of giant resonance (GR) [2]. The GDR is an oscillation of protons against neutrons represented as $\Delta T_z = 0$ and can be seen in a wider perspective when it is considered as a single component $\Delta T_z = 0$ of the IV dipole modes [3–6]. The additional components $\Delta T_z = \pm 1$ represent the charge-exchange modes. In addition to the Coulomb potential, with the presence of excess neutrons, *i.e.*, deformation in isospin space, the IV strengths reveal the splitting for $\Delta T_z = 0, \pm 1$ [3]. The charge-exchange excitations have attracted interest not only because they reflect the isospin and spin–isospin character of a nucleus but because they have a relevance for nuclear β -decay, thus connecting strong and weak interactions [7]. However, there has been little study of the giant multipole resonances other than the dipole, isobaric

analog (IAR), and Gamow–Teller (GTR) resonances [1].

Extensive theoretical works in Refs. [4–6] opened up an avenue of the study for the IV multipole excitations other than $\Delta L = 1$. Recent experimental progress has enabled precise measurements of the electric quadrupole resonance [8], which is instrumental for understanding the nuclear symmetry energy [9]. Furthermore, not only light-ion but heavy-ion charge-exchange reactions have become an effective probe for investigating the multipole excitations, which the nucleonic probes are difficult to study [10]. Despite the experimental advances, most of the theoretical studies have been mostly restricted to spherical nuclei except some attempts [11–14] though $\Delta T_z = 0$ and $\Delta S = 0$.

The nuclear shape deformation brings about a characteristic feature in the GRs; peak splitting of the GDR, which is caused by the different frequencies of oscillation along the long and short axes, has been observed in experiments [2]. The splitting of the distribution of the strengths has also been investigated in the isoscalar (IS) giant multipole resonances represented as $\Delta T = 0$, which is another branch of the GRs [1]. For the monopole $\Delta L = 0$ resonance, the spitting is due to the coupling to the $\Delta L_z = 0$ component of the quadrupole $\Delta L = 2$ resonance [15], which manifests the breaking of the rotational symmetry in the intrinsic frame.

The present work aims to provide a consistent and systematic description of all three modes $\Delta T_z = 0, \pm 1$ of IV excitations for both electric $\Delta S = 0$ and magnetic $\Delta S = 1$ types in a single framework, and to study the spitting of the distribution of the strengths according to ΔT_z and ΔL_z or ΔJ_z associated with deforma-

* E-mail: kyoshida@ruby.scphys.kyoto-u.ac.jp

tion in isospin space and real space. Thus, I consider open-shell nuclei where the nuclear deformation occurs in the ground state after demonstrating that the present framework describes the IV responses in spherical nuclei. I use a nuclear energy-density-functional (EDF) method: a theoretical model being capable of handling nuclides with arbitrary mass numbers [16, 17],

This paper is organized in the following way: the theoretical framework for describing the nuclear responses is given in Sec. II and the detail of the numerical procedures is also given; Sec. III is devoted to the numerical results and discussion based on the model calculation; non-spin flip electric-type excitations and spin-flip magnetic-type excitations are discussed in Sec. III A and Sec. III B, respectively; then, a summary is given in Sec. IV.

II. THEORETICAL MODEL

A. KSB and QRPA calculations

Since the details of the formalism can be found in Refs. [12, 18–20], here I briefly recapitulate the basic equations relevant to the present study. In the framework of the nuclear EDF method I employ, the ground state of a mother (target) nucleus is described by solving the Kohn–Sham–Bogoliubov (KSB) equation [21]:

$$\sum_{s'} \begin{bmatrix} h_{ss'}^q(\mathbf{r}) - \lambda^q \delta_{ss'} & \tilde{h}_{ss'}^q(\mathbf{r}) \\ \tilde{h}_{ss'}^q(\mathbf{r}) & -h_{ss'}^q(\mathbf{r}) + \lambda^q \delta_{ss'} \end{bmatrix} \begin{bmatrix} \varphi_{1,\alpha}^q(\mathbf{r}s') \\ \varphi_{2,\alpha}^q(\mathbf{r}s') \end{bmatrix} = E_\alpha \begin{bmatrix} \varphi_{1,\alpha}^q(\mathbf{r}s) \\ \varphi_{2,\alpha}^q(\mathbf{r}s) \end{bmatrix}, \quad (1)$$

where the single-particle and pair Hamiltonians, $h_{ss'}^q(\mathbf{r})$ and $\tilde{h}_{ss'}^q(\mathbf{r})$, are given by the functional derivative of the EDF with respect to the particle density and the pair density, respectively. An explicit expression of the Hamiltonians is found in the Appendix of Ref. [22]. The superscript q denotes ν (neutron, $t_z = 1/2$) or π (proton, $t_z = -1/2$). The average particle number is fixed at the desired value by adjusting the chemical potential λ^q . Assuming the system is axially symmetric, the KSB equation (1) is block diagonalized according to the quantum number Ω , the z -component of the angular momentum.

The excited states $|i\rangle$ are described as one-phonon excitations built on the ground state $|0\rangle$ of the mother nucleus as

$$|i\rangle = \hat{\Gamma}_i^\dagger |0\rangle, \quad (2)$$

$$\hat{\Gamma}_i^\dagger = \sum_{\alpha\beta} \left\{ X_{\alpha\beta}^i \hat{a}_\alpha^\dagger \hat{a}_\beta^\dagger - Y_{\alpha\beta}^i \hat{a}_\beta \hat{a}_\alpha \right\}, \quad (3)$$

where \hat{a}^\dagger and \hat{a} are the quasiparticle (qp) creation and annihilation operators that are defined in terms of the solutions of the KSB equation (1) with the Bogoliubov transformation. The phonon states, the amplitudes X^i, Y^i

and the vibrational frequency ω_i , are obtained in the quasiparticle-random-phase approximation (QRPA): the linearized time-dependent density-functional theory for superfluid systems [17]. The EDF gives the residual interactions entering into the QRPA equation. For the axially symmetric nuclei, the QRPA equation is block diagonalized according to the quantum number $K = \Omega_\alpha + \Omega_\beta$.

B. Numerical procedures

I solve the KSB equation in the coordinate space using cylindrical coordinates $\mathbf{r} = (\varrho, z, \phi)$. Since I assume further the reflection symmetry, only the region of $z \geq 0$ is considered. I use a two-dimensional lattice mesh with $\varrho_i = (i - 1/2)h$, $z_j = (j - 1)h$ ($i, j = 1, 2, \dots$) with a mesh size of $h = 0.6$ fm and 25 points for each direction. The qp states are truncated according to the qp energy cutoff at 60 MeV, and the qp states up to the magnetic quantum number $\Omega = 23/2$ with positive and negative parities are included. I introduce the truncation for the two-quasiparticle (2qp) configurations in the QRPA calculations, in terms of the 2qp-energy as 70 MeV.

For the normal (particle–hole) part of the EDF, I employ the SkM* functional [23]. For the pairing energy, I adopt the so-called mixed-type interaction:

$$V_{\text{pair}}^q(\mathbf{r}, \mathbf{r}') = V_0 \left[1 - \frac{\rho(\mathbf{r})}{2\rho_0} \right] \delta(\mathbf{r} - \mathbf{r}') \quad (4)$$

with $\rho_0 = 0.16 \text{ fm}^{-3}$, and $\rho(\mathbf{r})$ being the isoscalar (matter) particle density. I use the parameter V_0 as fixed in the previous studies: $V_0 = -275 \text{ MeV fm}^3$ for the Mg and Si isotopes [24], $V_0 = -240 \text{ MeV fm}^3$ for the Ni, Zr, and Pb isotopes [11]. For the pairing energy of the Sm isotopes, I adopt the one in Ref. [25] that depends on both the IS and IV densities, in addition to the pair density, with the parameters given in Table III of Ref. [25]. The same pair interaction is employed for the dynamical pairing in the QRPA calculation and for the $S = 0$ and $S = 1$ proton–neutron-pairing in the pnQRPA calculation, while the linear term in the IV density is dropped. Note that the pnQRPA calculations including the dynamic spin-triplet pairing with more or less the same strength as the spin-singlet pairing describe well the characteristic low-lying Gamow–Teller strength distributions in the light $N \simeq Z$ nuclei [26–28], and the β -decay half-lives of neutron-rich Ni isotopes [29]. Furthermore, the present theoretical framework describes well the measured giant resonances in light, medium-heavy, and heavy nuclei [12, 24, 30–36], and low-lying collective modes of vibration [12, 37–41].

III. RESULTS AND DISCUSSION

A. Electric modes: Non-spin-flip excitations

I consider the response to the IV operators defined by

$$\hat{F}_{LK\mu}^{(e)} = \frac{1}{\sqrt{2}} \sum_{ss'} \sum_{tt'} \int d\mathbf{r} f(r) Y_{LK}(\hat{r}) \delta_{ss'} \langle t' | \tau_\mu | t \rangle \times \hat{\psi}^\dagger(\mathbf{r}s't') \hat{\psi}(\mathbf{r}st), \quad (5)$$

where $\hat{\psi}^\dagger(\mathbf{r}st)$, $\hat{\psi}(\mathbf{r}st)$ represent the nucleon field operators, and $\vec{\tau} = (\tau_{+1}, \tau_0, \tau_{-1})$ denotes the spherical components of the Pauli matrix of isospin. I take $f(r) = \sqrt{4\pi}$ for the Fermi (F, $L = 0$) transition, while r^2 for the monopole (M, $L = 0$) and quadrupole (Q, $L = 2$) transitions.

1. Spherical nuclei

Before investigating deformed nuclei, I study the IV giant resonances in some spherical nuclei, where the experimental data are available. Figure 1 shows the transition-strength distributions in ^{60}Ni , ^{90}Zr , and ^{208}Pb as an example of spherical nuclei:

$$S_L^\mu(E) = \sum_K \frac{dB(E, F_{LK\mu})}{dE}, \quad (6)$$

$$\frac{dB(E, F_{LK\mu})}{dE} = \frac{2E\gamma}{\pi} \sum_i \frac{\tilde{E}_i |\langle i | \hat{F}_{LK\mu}^{(e)} | 0 \rangle|^2}{(E^2 - \tilde{E}_i^2)^2 + E^2\gamma^2}, \quad (7)$$

where $\tilde{E}_i^2 = (\hbar\omega_i)^2 + \gamma^2/4$ [3]. The smearing width γ is set to 2 MeV, which is supposed to simulate the spreading effect, Γ^\downarrow , missing in the QRPA. For the charge-exchange modes of excitation, the excitation energy with respect to the ground state of the mother nucleus is evaluated by replacing E by $E \pm (\lambda^\nu - \lambda^\pi)$ for the $\mu = \pm 1$ channel [42]. Furthermore, in plotting the strength distributions with respect to the ground state of the daughter nucleus, the mass difference between the mother and daughter is considered by using AME2020 [43, 44]: the ground-state Q value is -6.1 MeV and -2.8 MeV in ^{60}Cu and ^{60}Co with respect to ^{60}Ni , -6.1 MeV and -2.2 MeV in ^{90}Nb and ^{90}Y with respect to ^{90}Zr , and -2.9 MeV and -5.0 MeV in ^{208}Bi and ^{208}Tl with respect to ^{208}Pb .

A striking feature one sees in the $\mu = -1$ channel is the concentration of the monopole strength in the isobaric analog resonance (IAR). I find 53%, 68%, and 85% of the total strength in the IAR in ^{60}Cu , ^{90}Nb , and ^{208}Bi , respectively, as summarized in Tab. I. It is noted that the summed strengths excluding the IAR are given in the parenthesis in Tab. I. A similar trait was also found in the early investigation [4]. In the high-frequency region, the peak energy of the monopole resonance is higher than the quadrupole resonance. This is also the case in the $\mu = 0$ and $\mu = +1$ channels. Furthermore, the strengths are

spread out over a wider energy region for the monopole resonance; the width of the IVGMR is larger than that of the IVGQR.

Table I lists the summed strengths for the monopole and quadrupole excitations. One can see that the present calculation satisfies the model-independent non-energy weighted sum rule for the charge-exchange modes [3]:

$$m_L^{-1} - m_L^{+1} = \begin{cases} N - Z & \text{F} \\ \frac{2L+1}{4\pi} (N \langle r^4 \rangle_\nu - Z \langle r^4 \rangle_\pi) & \text{M, Q} \end{cases}, \quad (8)$$

where $\langle \dots \rangle_{\nu(\pi)}$ stands for the expectation value evaluated for neutrons (protons) in the ground state of the mother nucleus, and

$$m_L^\mu = \int dE S_L^\mu(E). \quad (9)$$

In these nuclei, m^{-1} is always larger than m^{+1} because $\langle r^4 \rangle$ for neutrons is slightly larger than that for protons. The monopole and quadrupole excitations are primarily built of a coherent particle-hole configurations of $2\hbar\omega_0$ excitation, and the high-frequency resonance is such a mode of excitation. However, the $0\hbar\omega_0$ excitation can also be involved.

For the monopole excitations, the $\nu 2p_{3/2} \rightarrow \pi 2p_{3/2}$ and $\nu 1g_{9/2} \rightarrow \pi 1g_{9/2}$ excitation generates the IAR of ^{60}Ni and ^{90}Zr , while the $0\hbar\omega_0$ excitation is strongly suppressed in the $\mu = 0$ and $+1$ channels due to the Pauli blocking. Therefore, the summed strength m^{-1} excluding the IAR has a similar value to m^0 and m^{+1} , which indicates that the higher-energy monopole strengths in the $\mu = -1$ channel represent the $2\hbar\omega_0$ excitation. In ^{208}Pb , no $0\hbar\omega_0$ excitation is available in the $\mu = 0$ and $\mu = +1$ channels as in ^{60}Ni and ^{90}Zr , and the summed strength m^{-1} excluding the IAR has a similar value to m^0 . However, the number of particle-hole configurations in the $\mu = +1$ channel and the m^{+1} value are smaller since the Fermi levels of neutrons and protons are located apart by $N = 1$.

The quadrupole excitation is more involved. In ^{60}Ni , the $1f_{7/2} \rightarrow 1f_{5/2}$ excitation is available in all the channels. The $\nu 1p_{3/2} \rightarrow \pi 1p_{3/2}$ excitation participates in the low-lying 2^+ excitation in the $\mu = -1$ channel, and the $1p_{3/2} \rightarrow 1p_{1/2}$ excitation further contribute to generate the 2^+ excitation in the $\mu = -1$ and $\mu = 0$ channels. Thus, the 2^+ states appear in low energy with the transition strengths dependent on μ . In ^{90}Zr , the $1g_{9/2} \rightarrow 1g_{7/2}$ excitation generates the low-lying 2^+ excitation in the $\mu = 0$ and $\mu = -1$ channel. Furthermore, the $\nu 1g_{9/2} \rightarrow \pi 1g_{9/2}$ excitation participates in the low-lying 2^+ excitation in the $\mu = -1$ channel. Therefore, one sees the strengths in low energy, while there are no strengths in the $\mu = +1$ channel since the $0\hbar\omega_0$ excitation is not available. In ^{208}Pb , both $0\hbar\omega_0$ and $2\hbar\omega_0$ excitations generate the 2^+ excitation in the $\mu = -1$ channel, acquiring a large strength. In the $\mu = 0$ channel,

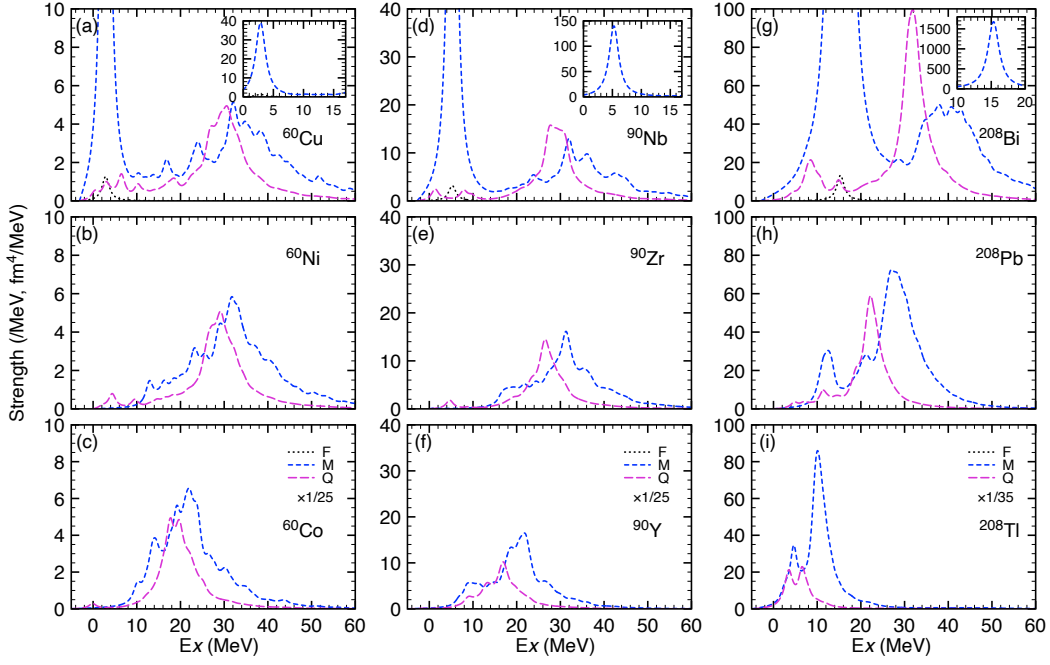


FIG. 1. Transition strengths of the non-spin-flip excitations in the $\mu = -1$ [(a), (d), (g)], $\mu = 0$ [(b), (e), (h)], and $\mu = +1$ channels [(c), (f), (i)]. The Fermi (F), monopole (M), and quadrupole (Q) strengths are shown by the dotted, dashed, and long-dashed lines, respectively. The quadrupole strengths are multiplied by $1/25$ ($1/35$ for ^{208}Bi , Pb , Tl). The excitation energies E_x are with respect to the ground state of the daughter nucleus.

TABLE I. Summed monopole and quadrupole strengths, and comparison with the non-energy-weighted sum rule (NEWSR) values, given in units of fm^4 . $\langle r^4 \rangle$ for neutrons (protons) is 276 (257) fm^4 , 444 (421) fm^4 , and 1284 (1114) fm^4 in ^{60}Ni , ^{90}Zr , and ^{208}Pb , respectively. The summed monopole strengths excluding the strength of the IAR are given in the parenthesis.

	m_L^{-1}	m_L^{+1}	m_L^0	$m_L^{-1} - m_L^{+1}$	NEWSR
^{60}Ni					
$L = 0$	228.3 (107.1)	97.00	107.3	131.3	131.1
$L = 2$	1901	1242	1546	658.6	655.4
^{90}Zr					
$L = 0$	639.2 (202.2)	212.2	217.8	427.0	425.8
$L = 2$	4427	2289	3259	2138	2129
^{208}Pb					
$L = 0$	6210 (952.3)	599.6	1044	5610	5607
$L = 2$	33734	5681	16063	28053	28036

the $\pi 1h_{11/2} \rightarrow \pi 1h_{9/2}$ and $\nu 1i_{13/2} \rightarrow \nu 1i_{11/2}$ excitations as well as the $2\hbar\omega_0$ excitation generate the 2^+ excitation. However, the $0\hbar\omega_0$ excitation is unavailable in the $\mu = +1$ channel. Therefore, the transition strengths in the $\mu = +1$ channel are smaller than in the other channels as in the monopole case.

Here, I compare the calculated strength distributions with the available experimental data. A systematic study of the charge-exchange (π^\pm, π^0) reaction reveals the IVGMR in medium-mass and heavy nuclei [45]: the excitation energy of the IVGMR measured using the $^{208}\text{Pb}(\pi^+, \pi^0)^{208}\text{Bi}$ reaction is 37.2 ± 3.5 MeV, while

$E_x = 12.0 \pm 2.8$ MeV in $^{208}\text{Pb}(\pi^-, \pi^0)^{208}\text{Tl}$. The excitation energy in lighter nuclei is $E_x = 35.6 \pm 2.8$ and 25.2 ± 1.7 MeV for ^{60}Cu and ^{60}Co , and $E_x = 34.6 \pm 2.9$ and 22.0 ± 2.0 MeV for ^{90}Nb and ^{90}Y . The inelastic electron scattering experiment suggests the resonance around 33 MeV in ^{208}Pb as the IVGMR [46], though this is ~ 5 MeV higher than the average of E_{T-1} and E_{T+1} obtained using the charge-exchange reaction. The nuclear reactions have also been employed to measure the IVGMR. The $\text{Pb}(^3\text{He}, tp)\text{Bi}$ reaction indicates the location of the IVGMR or spin monopole resonance at 30–45 MeV with respect to the ground state of Pb [47]. The IVGMR measured using the $(^7\text{Li}, ^7\text{Be})$ reaction is found at 20 ± 2 MeV in ^{60}Co [48]. In most cases, the present calculation describes well the location of the IVGMR.

The IVGQR has been found around $130 \times A^{-1/3}$ MeV in the $\mu = 0$ channel [1]. In ^{208}Pb , the excitation energy is 20–23 MeV [8, 49–51]. The IVGQR in ^{90}Zr is located around 26–27 MeV [52, 53]. The present calculation employing the SkM* functional reproduces well these experimental data. The $(^{13}\text{C}, ^{13}\text{N})$ reaction has been employed to locate the IVGQR in ^{60}Co , and it is found at $E_x = 20 \pm 2$ MeV [54]. The calculation is in remarkable agreement with the experiment, as shown in Fig. 1(c)

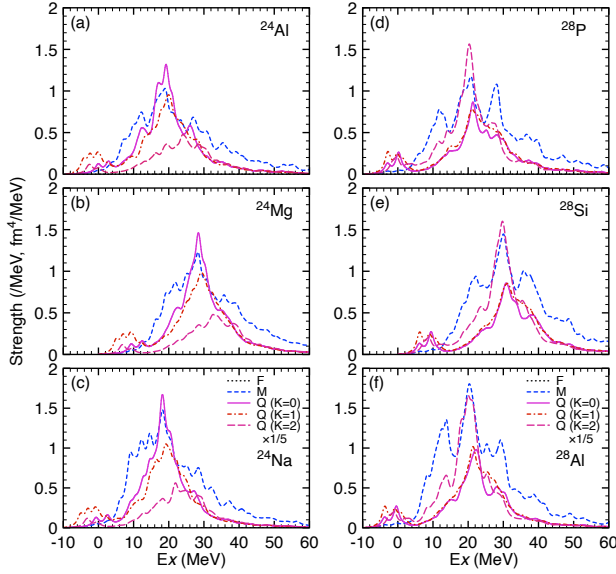


FIG. 2. As Fig. 1 but for the deformed ^{24}Mg and ^{28}Si nuclei. Instead of showing the total strengths, those for each K component are shown for the quadrupole excitations. The quadrupole strengths are multiplied by $1/5$.

2. Deformation effects

I am going to investigate the deformation effects. Figure 2 shows the transition-strength distributions in ^{24}Mg and ^{28}Si as an example of light deformed nuclei. As discussed in Refs. [24, 33–35], the ground state is prolately deformed and oblately deformed with the deformation parameter $\beta_2 = 0.39$ and -0.22 in ^{24}Mg and ^{28}Si , respectively. Since these nuclei have the same number of protons and neutrons, the Fermi transition strength is weak. A characteristic feature of these $N = Z$ nuclei is that the transition strength distributions in the three channels are similar to each other. For the dipole case, this characteristic trait has been discussed in Ref. [55]. Without the Coulomb potential, one cannot distinguish the motion of protons and neutrons in $N = Z$ nuclei, and the isotriplet states are degenerated. However, the Coulomb potential slightly expands the proton distribution, which leads to the asymmetry, as expected by the sum rule (8). A simple RPA analysis for a single normal mode employing the separable interaction gives the relation for the summed transition strengths as [3]

$$\frac{1}{2}(m^{-1} + m^{+1}) = \left[1 + O\left(\frac{N-Z}{A}\right) \right] m^0. \quad (10)$$

In deformed nuclei, the K -splitting occurs for the multipole modes of excitation, and thus the sum rule (8) for the quadrupole excitation is generalized by replacing $\langle r^4 \rangle$

TABLE II. As Tab. I for ^{24}Mg and ^{28}Si .

	m_L^{-1}	m_L^{+1}	m_L^0	$m_L^{-1} - m_L^{+1}$	NEWSR
^{24}Mg					
$L = 0$	23.27	29.25	26.20	-5.98	-6.01
$L = 2, K = 0$	86.94	95.77	91.40	-8.83	-8.93
$L = 2, K = 1$	80.47	87.56	84.32	-7.09	-7.18
$L = 2, K = 2$	45.32	48.68	47.04	-3.36	-3.39
^{28}Si					
$L = 0$	26.82	34.67	30.66	-7.84	-7.87
$L = 2, K = 0$	65.43	71.66	68.64	-6.23	-6.29
$L = 2, K = 1$	73.32	79.62	76.54	-6.30	-6.35
$L = 2, K = 2$	93.86	104.0	99.02	-10.12	-10.18

with

$$\begin{aligned} \frac{5}{4} \langle 4z^4 + \rho^4 - 4\rho^2 z^2 \rangle & \quad Q(K=0) \\ \frac{1}{15} \langle \rho^2 z^2 \rangle & \quad Q(K=\pm 1) \\ \frac{2}{15} \langle \rho^4 \rangle & \quad Q(K=\pm 2) \end{aligned} \quad (11)$$

depending on the K quantum number. Table II summarizes the summed strengths in ^{24}Mg and ^{28}Si , and the NEWSR values taking the nuclear deformation into account (11). One finds that in both nuclei the relation (10) holds accurately. It should be noted that the relation (10) is model dependent. However, the present selfconsistent model satisfies the simple relation, suggesting a rather generous rule for the IV excitations.

As mentioned above, the ^{24}Mg and ^{28}Si nuclei have different shapes in the ground states: prolate deformation in ^{24}Mg and oblate deformation in ^{28}Si . As a consequence of the prolate (oblate) deformation, distinctive features show up in the quadrupole strength distributions in high energy. The $K = 0$ ($K = 2$) states move toward low energy and acquire more considerable strengths in the prolately (oblately) deformed configuration. Furthermore, the coupling to the $K = 0$ component of the IVGQR brings about the resonance peak in the IVGMR. These features are common to the IS excitation. The enhancement of the $K = 0$ ($K = 2$) strengths in the prolate (oblate) configuration, which is also seen in Tab. II, may be understood by looking at the summed strengths (11). In a prolately (oblately) deformed state, $\langle z^4 \rangle$ increases (decreases), while $\langle \rho^4 \rangle$ decreases (increases), though the evaluation of $\langle \rho^2 z^2 \rangle$ requires a detail of the density distribution.

In Ref. [56], the $^{28}\text{Si}(^{10}\text{Be}, ^{10}\text{B}^*)$ reaction has been employed to identify the IVGMR in a deformed nucleus. The differential cross-section displays a broad peak ranging from 10 MeV to 30 MeV in ^{28}Al . The present calculation reasonably explains the measurement. However, it is not easy to find unique features due to deformation as the strength distribution is spread over a wide energy range.

The coupling between the GMR and the $K = 0$ component of the GQR becomes strong in a strongly deformed

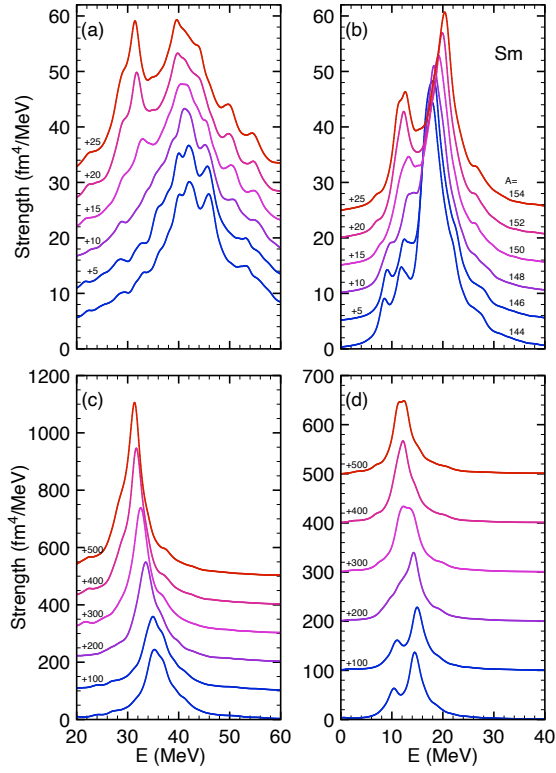


FIG. 3. Monopole strengths in the (a) $\mu = -1$ channel and (b) $\mu = +1$ channel of the Sm isotopes (shifted), and the $K = 0$ component of quadrupole strength distributions in the (c) $\mu = -1$ channel and (d) $\mu = +1$ channel (shifted). The excitation energies are with respect to the ground state of the target nuclei.

nucleus, which has been investigated for the ISGMR in detail from light to medium-heavy nuclei [15]. The deformation effect on the coupling has also been investigated theoretically for the IVGMR [11, 12]: in the $\mu = 0$ channel, the IVGMR shows up at about 30 MeV and the IVGQR around 25 MeV in the Nd and Sm isotopes; see Figs. 6(b) and 6(d) of Ref. [12]. In ^{154}Sm , which is strongly deformed, a resonance peak appears around 20 MeV and one finds clearly the splitting of the monopole strengths [12]. Because the study in Ref. [12] is restricted to the $\mu = 0$ channel, I am going to investigate the deformation effect on the coupling in the $\mu = \pm 1$ channels and to see the coupling between the GMR and the $K = 0$ component of the GQR is a general feature emerging in deformed nuclei.

Figures 3(a) and 3(b) show the monopole strength distributions in the $\mu = -1$ and $\mu = +1$ channels of the Sm isotopes. Here, the excitation energies are with respect to the ground state of the targets: the Sm isotopes. The IARs are excluded in plotting the strength distribution for the monopole strengths in the $\mu = -1$ channel, because most of the strengths are found in the IAR. One sees that a lower-energy resonance shows up around 30 MeV in $^{150,152,154}\text{Sm}$, while there appears a

resonance around 40–50 MeV in all the isotopes, which is considered as a primal IVGMR. The SkM* functional produces the onset of quadrupole deformation in between $N = 84$ and 86, and the deformation gradually develops with an increase in the neutron number [31]. The stronger the ground-state deformation, the more enhanced the transition strengths in the lower energy region. The $K = 0$ component of the quadrupole strengths is shown in Fig. 3(c). One finds that the monopole resonance in low energy is strongly coupled with the $K = 0$ component of the IVGQR in the well-deformed isotopes.

A similar feature can be seen in the $\mu = +1$ channel: one sees a resonance around 20–25 MeV in all the Sm isotopes, and a prominent peak appears in $^{152,154}\text{Sm}$ in low energy at ~ 10 –15 MeV. The $K = 0$ component of the IVGQR in these isotopes has a peak around 10–15 MeV, as shown in Fig. 3(d), where the lower-energy resonance of the monopole strengths shows up.

B. Magnetic modes: Spin-flip excitations

Here, I consider the response to the IV operators defined by

$$\hat{F}_{JK\mu}^{(m)} = \frac{1}{\sqrt{2}} \sum_{ss'} \sum_{tt'} \int d\mathbf{r} f(r) [Y_L \otimes \vec{\sigma}]_K^J \langle t' | \tau_\mu | t \rangle \times \hat{\psi}^\dagger(\mathbf{r}s't') \hat{\psi}(\mathbf{r}st), \quad (12)$$

where $[Y_L \otimes \vec{\sigma}]_K^J = \sum_{\nu\nu'} \langle L\nu 1\nu' | JK \rangle Y_{L\nu}(\hat{r}) \langle s' | \sigma_{\nu'} | s \rangle$ with the spherical components of the Pauli spin matrix $\vec{\sigma} = (\sigma_{+1}, \sigma_0, \sigma_{-1})$. I take $f(r) = \sqrt{4\pi}$ for the GT ($L = 0$) transition, while r^2 for the monopole ($L = 0$) and quadrupole ($L = 2$) transitions as in the electric cases. The $J = 3$ spin-quadrupole (SQ) excitation in the $\mu = 0$ channel corresponds to the spin-M3 excitation apart from a factor.

1. Spin quadrupole excitations in spherical nuclei

Since there are plenty of studies on the GT and spin monopole (SM) responses in spherical nuclei, such as in Ref. [57] where the Skyrme EDF method has been applied to the SM excitations, I do not show similar results to Ref. [57], but rather I focus on the SQ excitations.

Figure 4 shows the transition-strength distributions in ^{90}Zr and ^{208}Pb as an example of spherical nuclei. As in the electric cases, the μ -dependence of the strength distribution is more substantial with increasing excess neutrons. In ^{90}Zr , the excitations are mainly built of the $2\hbar\omega_0$ excitation: $N = 3 \rightarrow 5$ and $N = 2 \rightarrow 4$. Among them, the $1f_{5/2} \rightarrow 1h_{11/2}$ excitation with $J = 3$ appears in low energy. In the $\mu = 0$ and -1 channels, the $0\hbar\omega_0$ excitation is also possible to occur: the particle-hole excitations from the $\nu 1g_{9/2}$ orbital within the $N = 4$ shell. Furthermore, the $\nu 1g_{9/2} \rightarrow \pi 1g_{9/2}$ excitation participates in forming the low-lying states in the $\mu = -1$

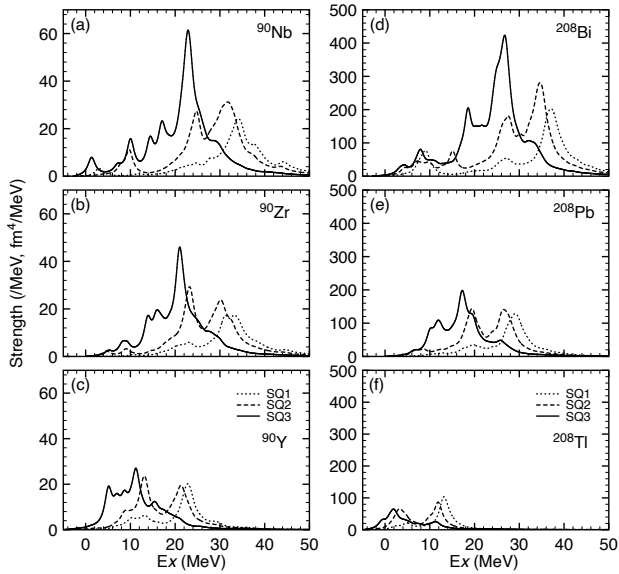


FIG. 4. As Fig. 1 but for the spin quadrupole (SQ) strengths. The $J = 1, 2$, and 3 states are depicted by the dotted, dashed, and solid lines, respectively.

channel. In ^{208}Pb , the $\pi 2d_{3/2} \rightarrow \nu 2g_{9/2}$ excitation with $J = 3$ and the $\pi 2d_{3/2} \rightarrow \nu 3d_{5/2}$ and $\pi 1h_{11/2} \rightarrow \nu 1j_{15/2}$ excitations generate the low energy states in the $\mu = +1$ channel. In the $\mu = 0$ and -1 channels, the $0\hbar\omega_0$ excitation is also available: the particle-hole excitations from the $\nu 1i_{13/2}$ orbital in the $N = 6$ shell. Furthermore, the $\nu 1h_{11/2} \rightarrow \pi 1h_{11/2}$ excitation participates in forming the low-lying states in the $\mu = -1$ channel.

In these examples, one sees that the excitation energy of $J = 3$ is the lowest and $J = 1$ the highest. This is already seen in the unperturbed strength distributions and is consistent with the finding in the early study [6]. This is partly because the $J = 3$ states are constructed by the particle-hole excitation of the orbitals with $(\ell - 2)_{j<}$ and $\ell_{j>}$, whose unperturbed energy is lowered by the spin-orbit interaction. This explanation is similar to that quoted for the lowering of the $J = 2$ states of the spin dipole excitations [58].

2. Deformation effects

I am going to investigate the deformation effects. Figure 5 shows the GT and SM transition-strength distributions in ^{24}Mg and ^{28}Si . The total strengths denoted by the solid lines include the GT and SM transitions to both the $J = 1$ states with $K = 0$ and those with $K = \pm 1$, while the dotted and dashed lines depict the $K = 0$ and $|K| = 1$ states, respectively. A large fraction of the SM strengths is found in low energy, where the GTR shows up. This characteristic feature is found in spherical nuclei as well [6, 57]. As in the electric cases, the transition strength distributions in the three channels are similar to

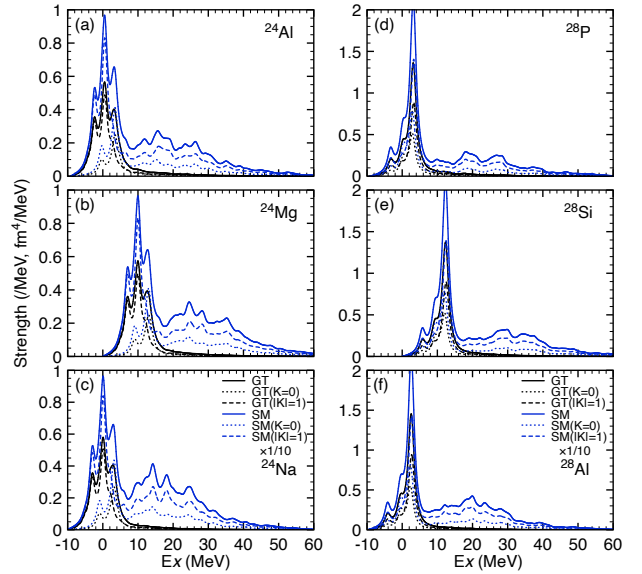


FIG. 5. As Fig. 2 but for the Gamow-Teller and spin-monopole (SM) excitations. The strengths of $K = \pm 1$ are summed for $|K| = 1$. The SM strengths are multiplied by $1/10$. The total strengths denoted by the solid lines include both the $J = 1$ states with $K = 0$ and those with $K = \pm 1$, while the dotted and dashed lines show the $K = 0$ and $|K| = 1$ states, respectively.

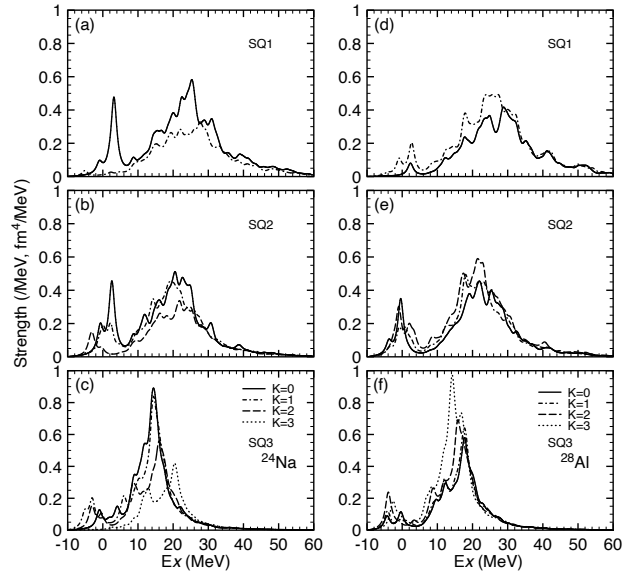


FIG. 6. As Fig. 2 but for the spin-quadrupole (SQ) excitations in the $\mu = +1$ channel.

each other. Furthermore, the SM transition strengths in the $\mu = +1$ channel are enhanced because the Coulomb potential slightly expands the proton distribution, which leads to the asymmetry even in the $N = Z$ nuclei.

The strength distributions for $K = 0$ and $K = 1$ are different since the ground state is deformed. However,

the K -splitting does not show a “universal behavior” that the $K = 0$ states are shifted lower (higher) in energy in a prolately (oblately) deformed nucleus. This is because the GT operator does not change the spatial structure and the SM operator does not depend on the spatial direction. Furthermore, the ground state is time-even: $\langle \sigma_\nu \rangle = 0$. The K -splitting occurring in the GT and SM excitations are due not to the collective deformation but to the underlying shell structure. In ^{24}Mg , the $K = 1$ states appear lower in energy than the $K = 0$ states, although the ground state is prolately deformed. The Fermi levels of neutrons and protons are both located in between the $[211]3/2$ and $[202]5/2$ orbitals. The $K = 1$ state is mainly generated by the $[211]3/2 \rightarrow [202]5/2$ and $[211]3/2 \rightarrow [211]1/2$ excitations, while the $K = 0$ state is constructed, *e.g.*, by the $[220]1/2 \rightarrow [211]1/2$ excitation, both of which are far from the Fermi level. Thus, the $K = 1$ states appear lower in energy.

I then investigate the SQ excitations. Since the SQ operator involves the spherical harmonics $Y_{2\nu}(\hat{r})$, the K -dependence can be attributed to nuclear deformation. However, the K quantum number is composed of the z -component of angular momentum, reflecting the nuclear shape, and intrinsic spin, it is not apparant to expect a direct correspondence between the K -splitting and the nuclear deformation.

As discussed so far, the strength distributions in the $\mu = 0$ and ± 1 channels are similar to each other for the $N = Z$ light nuclei. Thus, I show in Fig. 6 the transition-strength distribution in the $\mu = +1$ channel only. One sees that the distributions for each K are different. The $K = 0$ ($K = 1$) strengths are enhanced in a prolately (oblately) deformed nucleus for $J = 1$. A universal feature of the K -splitting can be seen for $J = 3$: the lower (higher)- K states appear lower in energy and possess enhanced strengths in a prolately (oblately) deformed nucleus. However, it is not easy to distinguish the strength distributions of each K for $J = 2$.

In the electric case, the K -dependence of the transition strengths was evaluated qualitatively by looking at the NEWSR values using Eq. (11). The NEWSR values for the GT and SM excitations are essentially the same as those assuming spherical symmetry (8): the spatial function $f(r)$ is constant for the GT operator, and that for the SM operator is r^2 , which is scalar. However, one needs to consider the K -dependence for the SQ excitations. The NEWSR for the SQ excitations with (J, K) reads

$$m_{L=2(J,K)}^{-1} - m_{L=2(J,K)}^{+1}$$

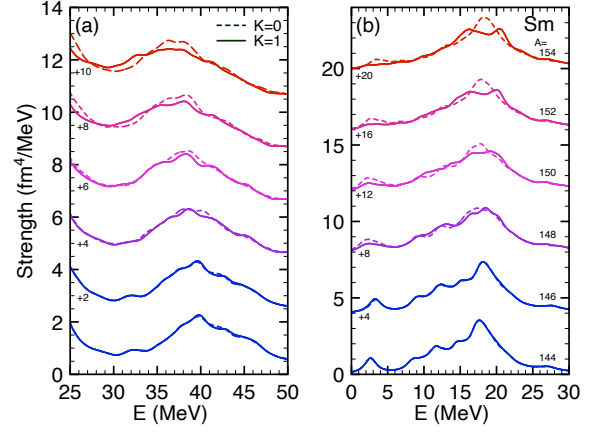


FIG. 7. As Fig. 3 but for the spin-monopole (SM) excitations. The strengths for $K = 0$ and $K = 1$ are separately depicted by the dashed and solid lines, respectively.

$$= \begin{cases} \frac{1}{8\pi} (N \langle 4z^4 + \rho^4 + 5\rho^2 z^2 \rangle_\nu - Z \langle \dots \rangle_\pi) & (1,0) \\ \frac{16\pi}{15} (N \langle 2z^4 + 5\rho^4 + 7\rho^2 z^2 \rangle_\nu - Z \langle \dots \rangle_\pi) & (1,1) \\ \frac{16\pi}{5} (N \langle \rho^2 z^2 \rangle_\nu - Z \langle \dots \rangle_\pi) & (2,0) \\ \frac{16\pi}{5} (N \langle 2z^4 + \rho^4 - \rho^2 z^2 \rangle_\nu - Z \langle \dots \rangle_\pi) & (2,1) \\ \frac{16\pi}{5} (N \langle \rho^4 + 2\rho^2 z^2 \rangle_\nu - Z \langle \dots \rangle_\pi) & (2,2) \\ \frac{16\pi}{1} (N \langle 12z^4 + 3\rho^4 \rangle_\nu - Z \langle \dots \rangle_\pi) & (3,0) \\ \frac{32\pi}{5} (N \langle 16z^4 + 5\rho^4 + 16\rho^2 z^2 \rangle_\nu - Z \langle \dots \rangle_\pi) & (3,1) \\ \frac{32\pi}{5} (N \langle \rho^4 + 8\rho^2 z^2 \rangle_\nu - Z \langle \dots \rangle_\pi) & (3,2) \\ \frac{32\pi}{15} (N \langle \rho^4 \rangle_\nu - Z \langle \dots \rangle_\pi) & (3,3) \end{cases}, \quad (13)$$

where $\langle \dots \rangle_\pi$ denotes the expectation value of the first term by replacing neutrons with protons. In deriving these sum rule values, I assume that J^π of the ground state of the mother nucleus is 0^+ : the time-odd densities vanish in the ground state. For $J = 1$, the $K = 0$ ($K = 1$) strengths are characterized by a large $\langle z^4 \rangle$ ($\langle \rho^4 \rangle$) term. Since the prolate (oblate) deformation produces the large $\langle z^4 \rangle$ ($\langle \rho^4 \rangle$) value, the above finding can be reasonably understood. The ‘stretched’ $J = 3$ excitation is relatively simple, particularly the $K = 0$ and $K = 3$ states. The prolate (oblate) deformation gives larger strengths in the $K = 0$ ($K = 3$) states. A similar feature has been found in the ‘stretched’ $J = 2$ spin-dipole excitation in deformed nuclei though the K -dependence is not clear for the $J = 0$ and $J = 1$ excitations [55].

According to the coupling between the monopole and the $K = 0$ component of the quadrupole excitations seen in the electric case, which is universal both in the IS and IV excitations, one is tempted to expect the spitting of the SM strengths to appear due to coupling to the $K = 0$ and $K = 1$ components of the SQ excitations in deformed

nuclei. Figure 7 shows the SM transition strengths in the Sm isotopes with $A = 144$ –154. Here, the $K = 0$ and $K = 1$ strengths are displayed separately. It is hard to see the deformation effects in these distributions either in the $\mu = +1$ and $\mu = -1$ channels. One reason is that for the electric quadrupole excitations, the $K = 0$ strengths are concentrated in a single peak; however, in the current case, the $K = 0$ and $K = 1$ strengths of the SQ excitations are widely spread out in 30–40 MeV depending on J . Another reason is that the SM strengths distribution is broadened irrespective of the nuclear shape.

IV. SUMMARY

I have investigated the electric (non spin-flip) and magnetic (spin-flip) IV monopole and quadrupole modes of excitation. To obtain the generic features of the IV excitations, the neutral ($\mu = 0$) and charge-exchange ($\mu = \pm 1$) channels have been considered simultaneously. Furthermore, I have explored open-shell nuclei to obtain unique features associated with nuclear deformation. To this end, I employed the nuclear energy-density functional (EDF) method: the Skyrme–Kohn–Sham–Bogoliubov and the quasiparticle random-phase approximation were used to describe the ground state and the transition to excited states.

A strong concentration of the monopole strengths in the energy region of the IAR has been found regardless of nuclear deformation. In addition, a resonance structure appears in high energy, which is generated mainly by

particle–hole configurations with $2\hbar\omega_0$ excitation. The K -splitting occurs in the electric quadrupole excitations due to deformation. The lower (higher) K states appear lower (higher) in energy in a prolately deformed nucleus: the opposite in an oblatelly deformed nucleus. Thus, the K -splitting of the GQR is universal in the IS and IV excitations. Furthermore, the coupling to the $K = 0$ component of the GQR brings about the splitting of the monopole strengths in all the channels of IV excitation.

Similarly to the electric excitations, I have found a strong concentration of the spin-monopole strengths in the energy region of the GTR regardless of nuclear deformation. The $J = 3$ states appear lowest in energy among the spin-quadrupole resonances. The K -splitting occurs in the spin-monopole and spin-quadrupole excitations. However, the relation between the energy-ordering depending on K and the deformation is not apparent: the K splitting in the spin-monopole excitation is due to the change in the underlying shell structure similarly to the GTR, and that in the $J = 3$ spin-quadrupole resonance follows the universal trend.

ACKNOWLEDGMENTS

This work was supported by the JSPS KAKENHI (Grants No. JP19K03824 and No. JP19K03872). The numerical calculations were performed on Yukawa-21 at the Yukawa Institute for Theoretical Physics, Kyoto University.

-
- [1] M. Harakeh and A. Woude, *Giant Resonances: Fundamental High-frequency Modes of Nuclear Excitation*, Oxford Science Publications (Oxford University Press, Oxford, 2001).
 - [2] B. L. Berman and S. C. Fultz, Measurements of the giant dipole resonance with monoenergetic photons, *Rev. Mod. Phys.* **47**, 713 (1975).
 - [3] A. Bohr and B. Mottelson, *Nuclear Structure: Volume II, Nuclear Deformations* (Benjamin, Reading, MA, 1975).
 - [4] N. Auerbach and A. Klein, A microscopic theory of giant electric isovector resonances, *Nucl. Phys. A* **395**, 77 (1983).
 - [5] T. Izumoto, Giant spin-isospin vibrations and the continuum spectra from the (p,n) reaction at forward angles, *Nucl. Phys. A* **395**, 189 (1983).
 - [6] N. Auerbach and A. Klein, Structure of isovector spin excitations in nuclei, *Phys. Rev. C* **30**, 1032 (1984).
 - [7] F. Osterfeld, Nuclear spin and isospin excitations, *Rev. Mod. Phys.* **64**, 491 (1992).
 - [8] S. S. Henshaw, M. W. Ahmed, G. Feldman, A. M. Nathan, and H. R. Weller, New Method for Precise Determination of the Isovector Giant Quadrupole Resonances in Nuclei, *Phys. Rev. Lett.* **107**, 222501 (2011).
 - [9] X. Roca-Maza, M. Brenna, B. K. Agrawal, P. F. Bortignon, G. Colò, L.-G. Cao, N. Paar, and D. Vretenar, Giant Quadrupole Resonances in ^{208}Pb , the nuclear symmetry energy and the neutron skin thickness, *Phys. Rev. C* **87**, 034301 (2013), [arXiv:1212.4377 \[nucl-th\]](#).
 - [10] H. Lenske, F. Cappuzzello, M. Cavallaro, and M. Colonna, Heavy ion charge exchange reactions as probes for nuclear β -decay, *Prog. Part. Nucl. Phys.* **109**, 103716 (2019).
 - [11] K. Yoshida, Roles of deformation and neutron excess on the giant monopole resonance in neutron-rich Zr isotopes, *Phys. Rev. C* **82**, 034324 (2010), [arXiv:1008.1522 \[nucl-th\]](#).
 - [12] K. Yoshida and T. Nakatsukasa, Shape evolution of giant resonances in Nd and Sm isotopes, *Phys. Rev. C* **88**, 034309 (2013), [arXiv:1305.6437 \[nucl-th\]](#).
 - [13] G. Scamps and D. Lacroix, Systematic study of isovector and isoscalar giant quadrupole resonances in normal and superfluid deformed nuclei, *Phys. Rev. C* **89**, 034314 (2014), [arXiv:1401.5211 \[nucl-th\]](#).
 - [14] M. Kortelainen, N. Hinohara, and W. Nazarewicz, Multipole modes in deformed nuclei within the finite amplitude method, *Phys. Rev. C* **92**, 051302 (2015), [arXiv:1509.02353 \[nucl-th\]](#).
 - [15] U. Garg and G. Colò, The compression-mode giant resonances and nuclear incompressibility, *Prog. Part. Nucl. Phys.* **101**, 55 (2018), [arXiv:1801.03672 \[nucl-ex\]](#).

- [16] M. Bender, P.-H. Heenen, and P.-G. Reinhard, Self-consistent mean-field models for nuclear structure, *Rev. Mod. Phys.* **75**, 121 (2003).
- [17] T. Nakatsukasa, K. Matsuyanagi, M. Matsuo, and K. Yabana, Time-dependent density-functional description of nuclear dynamics, *Rev. Mod. Phys.* **88**, 045004 (2016), [arXiv:1606.04717](#).
- [18] K. Yoshida and N. Van Giai, Deformed quasiparticle-random-phase approximation for neutron-rich nuclei using the Skyrme energy density functional, *Phys. Rev. C* **78**, 064316 (2008), [arXiv:0809.0169 \[nucl-th\]](#).
- [19] K. Yoshida, Spin-isospin response of deformed neutron-rich nuclei in a self-consistent Skyrme energy-density-functional approach, *Prog. Theor. Exp. Phys.* **2013**, 113D02 (2013), [arXiv:1308.0424 \[nucl-th\]](#).
- [20] K. Yoshida, Erratum: Spin-isospin response of deformed neutron-rich nuclei in a self-consistent Skyrme energy-density-functional approach, *Prog. Theor. Exp. Phys.* **2021**, 019201 (2021).
- [21] J. Dobaczewski, H. Flocard, and J. Treiner, Hartree-Fock-Bogolyubov description of nuclei near the neutron drip line, *Nucl. Phys. A* **422**, 103 (1984).
- [22] H. Kasuya and K. Yoshida, Hartree-Fock-Bogoliubov theory for odd-mass nuclei with a time-odd constraint and application to deformed halo nuclei, *Prog. Theor. Exp. Phys.* **2021**, 013D01 (2021), [arXiv:2005.03276 \[nucl-th\]](#).
- [23] J. Bartel, P. Quentin, M. Brack, C. Guet, and H.-B. Håkansson, Towards a better parametrisation of Skyrme-like effective forces: A critical study of the SkM force, *Nucl. Phys. A* **386**, 79 (1982).
- [24] T. Peach, U. Garg, Y. K. Gupta, J. Hoffman, J. T. Matta, D. Patel, P. V. M. Rao, K. Yoshida, M. Itoh, M. Fujiwara, K. Hara, H. Hashimoto, K. Nakanishi, M. Yosoi, H. Sakaguchi, S. Terashima, S. Kishi, T. Murakami, M. Uchida, Y. Yasuda, H. Akimune, T. Kawabata, M. N. Harakeh, and G. Colò, Effect of ground-state deformation on isoscalar giant resonances in ^{28}Si , *Phys. Rev. C* **93**, 064325 (2016).
- [25] M. Yamagami, Y. Shimizu, and T. Nakatsukasa, Optimal pair density functional for description of nuclei with large neutron excess, *Phys. Rev. C* **80**, 064301 (2009), [arXiv:0812.3197 \[nucl-th\]](#).
- [26] Y. Fujita, H. Fujita, T. Adachi, C. L. Bai, A. Algora, G. P. A. Berg, P. von Brentano, G. Colò, M. Csatlós, J. M. Deaven, E. Estevez-Aguado, C. Fransen, D. De Frenne, K. Fujita, E. Ganioglu, C. J. Guess, J. Gulyás, K. Hatanaka, K. Hirota, M. Honma, D. Ishikawa, E. Jacobs, A. Krasznahorkay, H. Matsubara, K. Matsuyanagi, R. Meharchand, F. Molina, K. Muto, K. Nakanishi, A. Negret, H. Okamura, H. J. Ong, T. Otsuka, N. Pietralla, G. Perdikakis, L. Popescu, B. Rubio, H. Sagawa, P. Sarriguren, C. Scholl, Y. Shimbara, Y. Shimizu, G. Susoy, T. Suzuki, Y. Tameshige, A. Tamii, J. H. Thies, M. Uchida, T. Wakasa, M. Yosoi, R. G. T. Zegers, K. O. Zell, and J. Zenihiro, Observation of Low- and High-Energy Gamow-Teller Phonon Excitations in Nuclei, *Phys. Rev. Lett.* **112**, 112502 (2014).
- [27] Y. Fujita, H. Fujita, T. Adachi, G. Susoy, A. Algora, C. L. Bai, G. Colò, M. Csatlós, J. M. Deaven, E. Estevez-Aguado, C. J. Guess, J. Gulyás, K. Hatanaka, K. Hirota, M. Honma, D. Ishikawa, A. Krasznahorkay, H. Matsubara, R. Meharchand, F. Molina, H. Nakada, H. Okamura, H. J. Ong, T. Otsuka, G. Perdikakis, B. Rubio, H. Sagawa, P. Sarriguren, C. Scholl, Y. Shimbara, E. J. Stephenson, T. Suzuki, A. Tamii, J. H. Thies, K. Yoshida, R. G. T. Zegers, and J. Zenihiro, High-resolution study of Gamow-Teller excitations in the $^{42}\text{Ca}(^3\text{He}, t)^{42}\text{Sc}$ reaction and the observation of a “low-energy super-Gamow-Teller state”, *Phys. Rev. C* **91**, 064316 (2015).
- [28] H. Fujita, Y. Fujita, Y. Utsuno, K. Yoshida, T. Adachi, A. Algora, M. Csatlós, J. M. Deaven, E. Estevez-Aguado, C. J. Guess, J. Gulyás, K. Hatanaka, K. Hirota, R. Hutton, D. Ishikawa, A. Krasznahorkay, H. Matsubara, F. Molina, H. Okamura, H. J. Ong, G. Perdikakis, B. Rubio, C. Scholl, Y. Shimbara, G. Susoy, T. Suzuki, A. Tamii, J. H. Thies, R. G. T. Zegers, and J. Zenihiro, Experimental study of Gamow-Teller transitions via the high-energy-resolution $^{18}\text{O}(^3\text{He}, t)^{18}\text{F}$ reaction: Identification of the low-energy “super” -Gamow-Teller state, *Phys. Rev. C* **100**, 034618 (2019).
- [29] K. Yoshida, Suddenly shortened half-lives beyond ^{78}Ni : $N = 50$ magic number and high-energy non-unique first-forbidden transitions, *Phys. Rev. C* **100**, 024316 (2019), [arXiv:1903.03310 \[nucl-th\]](#).
- [30] T. Nakatsukasa, P. Avogadro, S. Ebata, T. Inakura, and K. Yoshida, Self-consistent description of nuclear photoabsorption cross sections, *Acta Phys. Polon. B* **42**, 609 (2011), [arXiv:1101.3106 \[nucl-th\]](#).
- [31] K. Yoshida and T. Nakatsukasa, Dipole responses in Nd and Sm isotopes with shape transitions, *Phys. Rev. C* **83**, 021304 (2011), [arXiv:1008.1520 \[nucl-th\]](#).
- [32] K. Yoshida, N. Hinohara, and T. Nakatsukasa, Skyrme energy-density functional approach to collective dynamics, *J. Phys.: Conf. Ser.* **321**, 012017 (2011).
- [33] Y. Gupta, U. Garg, J. Matta, D. Patel, T. Peach, J. Hoffman, K. Yoshida, M. Itoh, M. Fujiwara, K. Hara, H. Hashimoto, K. Nakanishi, M. Yosoi, H. Sakaguchi, S. Terashima, S. Kishi, T. Murakami, M. Uchida, Y. Yasuda, H. Akimune, T. Kawabata, and M. Harakeh, Splitting of ISGMR strength in the light-mass nucleus ^{24}Mg due to ground-state deformation, *Phys. Lett. B* **748**, 343 (2015).
- [34] Y. Gupta, U. Garg, J. Matta, D. Patel, T. Peach, J. Hoffman, K. Yoshida, M. Itoh, M. Fujiwara, K. Hara, H. Hashimoto, K. Nakanishi, M. Yosoi, H. Sakaguchi, S. Terashima, S. Kishi, T. Murakami, M. Uchida, Y. Yasuda, H. Akimune, T. Kawabata, and M. Harakeh, Corrigendum to “Splitting of ISGMR strength in the light-mass nucleus ^{24}Mg due to ground-state deformation” [*Phys. Lett. B* 748 (2015) 343–346], *Phys. Lett. B* **751**, 597 (2015).
- [35] Y. K. Gupta, U. Garg, J. Hoffman, J. Matta, P. V. M. Rao, D. Patel, T. Peach, K. Yoshida, M. Itoh, M. Fujiwara, K. Hara, H. Hashimoto, K. Nakanishi, M. Yosoi, H. Sakaguchi, S. Terashima, S. Kishi, T. Murakami, M. Uchida, Y. Yasuda, H. Akimune, T. Kawabata, and M. N. Harakeh, Deformation effects on isoscalar giant resonances in ^{24}Mg , *Phys. Rev. C* **93**, 044324 (2016).
- [36] K. Yoshida, Isovector spin susceptibility: Isotopic evolution of collectivity in spin response, (2021), [*Phys. Rev. C* (in press)], [arXiv:2103.16119 \[nucl-th\]](#).
- [37] K. Yoshida, Skyrme-QRPA calculations for low-lying excitation modes in deformed neutron-rich nuclei, *Eur. Phys. J. A* **42**, 583 (2009), [arXiv:0902.3053 \[nucl-th\]](#).
- [38] K. Yoshida and H. Watanabe, Enhanced collectivity of γ vibration in neutron-rich Dy isotopes with $N =$

- 108–110, *Prog. Theor. Exp. Phys.* **2016**, 123D02 (2016), [arXiv:1607.07111 \[nucl-th\]](#).
- [39] H. Watanabe, G. Zhang, K. Yoshida, P. Walker, J. Liu, J. Wu, P. Regan, P.-A. Söderström, H. Kanaoka, Z. Korkulu, P. Lee, S. Nishimura, A. Yagi, D. Ahn, T. Alharbi, H. Baba, F. Browne, A. Bruce, R. Carroll, K. Chae, Z. Dombradi, P. Doornenbal, A. Estrade, N. Fukuda, C. Griffin, E. Ideguchi, N. Inabe, T. Isobe, S. Kanaya, I. Kojouharov, F. Kondev, T. Kubo, S. Kubono, N. Kurz, I. Kuti, S. Lalkovski, G. Lane, C. Lee, E. Lee, G. Lorusso, G. Lotay, C.-B. Moon, I. Nishizuka, C. Nita, A. Odahara, Z. Patel, V. Phong, Z. Podolyák, O. Roberts, H. Sakurai, H. Schaffner, C. Shand, Y. Shimizu, T. Sumikama, H. Suzuki, H. Takeda, S. Terashima, Z. Vajta, J. Valiente-Dóbon, and Z. Xu, Long-lived K isomer and enhanced γ vibration in the neutron-rich nucleus ^{172}Dy : Collectivity beyond double midshell, *Phys. Lett. B* **760**, 641 (2016).
- [40] G. Zhang, H. Watanabe, G. Dracoulis, F. Kondev, G. Lane, P. Regan, P.-A. Söderström, P. Walker, K. Yoshida, H. Kanaoka, Z. Korkulu, P. Lee, J. Liu, S. Nishimura, J. Wu, A. Yagi, D. Ahn, T. Alharbi, H. Baba, F. Browne, A. Bruce, M. Carpenter, R. Carroll, K. Chae, C. Chiara, Z. Dombradi, P. Doornenbal, A. Estrade, N. Fukuda, C. Griffin, E. Ideguchi, N. Inabe, T. Isobe, S. Kanaya, I. Kojouharov, T. Kubo, S. Kubono, N. Kurz, I. Kuti, S. Lalkovski, T. Lauritsen, C. Lee, E. Lee, C. Lister, G. Lorusso, G. Lotay, E. McCutchan, C.-B. Moon, I. Nishizuka, C. Nita, A. Odahara, Z. Patel, V. Phong, Z. Podolyák, O. Roberts, H. Sakurai, H. Schaffner, D. Seweryniak, C. Shand, Y. Shimizu, T. Sumikama, H. Suzuki, H. Takeda, S. Terashima, Z. Vajta, J. Valiente-Dóbon, Z. Xu, and S. Zhu, Interplay of quasiparticle and vibrational excitations: First observation of isomeric states in ^{168}Dy and ^{169}Dy , *Phys. Lett. B* **799**, 135036 (2019).
- [41] K. Yoshida, Pairing and nonaxial-shape correlations in $N = 150$ isotones, (2021), [arXiv:2105.03128 \[nucl-th\]](#).
- [42] E. Yüksel, N. Paar, G. Colò, E. Khan, and Y. Niu, Gamow-Teller excitations at finite temperature: Competition between pairing and temperature effects, *Phys. Rev. C* **101**, 044305 (2020), [arXiv:1909.08930 \[nucl-th\]](#).
- [43] W. Huang, M. Wang, F. Kondev, G. Audi, and S. Naimi, The AME 2020 atomic mass evaluation (I). Evaluation of input data, and adjustment procedures, *Chin. Phys. C* **45**, 030002 (2021).
- [44] M. Wang, W. Huang, F. Kondev, G. Audi, and S. Naimi, The AME 2020 atomic mass evaluation (II). Tables, graphs and references, *Chin. Phys. C* **45**, 030003 (2021).
- [45] A. Erell, J. Alster, J. Lichtenstadt, M. A. Moinester, J. D. Bowman, M. D. Cooper, F. Irom, H. S. Matis, E. Pisasetzky, and U. Sennhauser, Measurements on isovector giant resonances in pion charge exchange, *Phys. Rev. C* **34**, 1822 (1986).
- [46] R. Pitthan, F. R. Buskirk, E. B. Dally, J. N. Dyer, and X. K. Maruyama, Electroexcitation of Giant Multipole Resonances in ^{197}Au and ^{208}Pb between 5 and 40 MeV Excitation Energy with 90-MeV Electrons, *Phys. Rev. Lett.* **33**, 849 (1974).
- [47] R. G. T. Zegers, A. M. van den Berg, S. Brandenburg, F. R. R. Fleurot, M. Fujiwara, J. Guillot, V. M. Hannen, M. N. Harakeh, H. Laurent, K. van der Schaaf, S. Y. van der Werf, A. Willis, and H. W. Wilschut, Search for Isovector Giant Monopole Resonances via the $\text{Pb}(^3\text{He}, tp)$ Reaction, *Phys. Rev. Lett.* **84**, 3779 (2000).
- [48] S. Nakayama, H. Akimune, Y. Arimoto, I. Daito, H. Fujimura, Y. Fujita, M. Fujiwara, K. Fushimi, H. Kohri, N. Koori, K. Takahisa, T. Takeuchi, A. Tamii, M. Tanaka, T. Yamagata, Y. Yamamoto, K. Yonehara, and H. Yoshida, Isovector Electric Monopole Resonance in ^{60}Ni , *Phys. Rev. Lett.* **83**, 690 (1999).
- [49] R. Leicht, M. Hammen, K. Schelhaas, and B. Ziegler, Absorption and scattering of photons by ^{208}Pb , *Nucl. Phys. A* **362**, 111 (1981).
- [50] K. Schelhaas, J. Henneberg, M. Sanzone-Arenhövel, N. Wieloch-Laufenberg, U. Zurmühl, B. Ziegler, M. Schumacher, and F. Wolf, Nuclear photon scattering by ^{208}Pb , *Nucl. Phys. A* **489**, 189 (1988).
- [51] D. S. Dale, R. M. Laszewski, and R. Alarcon, Isovector E2 resonance in ^{208}Pb , *Phys. Rev. Lett.* **68**, 3507 (1992).
- [52] S. Fukuda and Y. Torizuka, Evidence for the giant monopole resonance in ^{90}Zr , *Phys. Lett. B* **62**, 146 (1976).
- [53] M. A. Godwin, E. Hayward, G. Feldman, L. H. Kramer, H. R. Weller, and W. R. Dodge, Isovector giant quadrupole resonance observed in $^{89}\text{Y}(\bar{p}, \gamma)^{90}\text{Zr}$, *Phys. Rev. C* **50**, 1528 (1994).
- [54] T. Ichihara, M. Ishihara, H. Ohnuma, T. Niizeki, Y. Satou, H. Okamura, S. Kubono, M. H. Tanaka, and Y. Fuchi, Isovector Quadrupole Resonance Observed in the $^{60}\text{Ni}(^{13}\text{C}, ^{13}\text{N})^{60}\text{Co}$ Reaction at $E/A = 100$ MeV, *Phys. Rev. Lett.* **89**, 142501 (2002).
- [55] K. Yoshida, Charge-exchange dipole excitations in deformed nuclei, *Phys. Rev. C* **102**, 054336 (2020), [arXiv:2008.03947 \[nucl-th\]](#).
- [56] M. Scott, R. G. T. Zegers, R. Almus, S. M. Austin, D. Bazin, B. A. Brown, C. Campbell, A. Gade, M. Bowry, S. Galès, U. Garg, M. N. Harakeh, E. Kwan, C. Langer, C. Loelius, S. Lipschutz, E. Litvinova, E. Lunderberg, C. Morse, S. Noji, G. Perdikakis, T. Redpath, C. Robin, H. Sakai, Y. Sasamoto, M. Sasano, C. Sullivan, J. A. Tostevin, T. Uesaka, and D. Weisshaar, Observation of the Isovector Giant Monopole Resonance via the $^{28}\text{Si}(^{10}\text{Be}, ^{10}\text{B}^*[1.74\text{ MeV}])$ Reaction at 100 A MeV, *Phys. Rev. Lett.* **118**, 172501 (2017).
- [57] I. Hamamoto and H. Sagawa, Charge-exchange spin monopole modes, *Phys. Rev. C* **62**, 024319 (2000).
- [58] G. Bertsch, D. Cha, and H. Toki, Systematics of the $\sigma\tau$ -strength in nuclei, *Phys. Rev. C* **24**, 533 (1981).